The Astrophysical Journal, 902:107 (16pp), 2020 October 20 https://doi.org/10.3847/1538-4357/abb3fe

Assessing Spectroscopic Binary Multiplicity Properties Using Robo-AO Imaging

Stefan Laos[1], Keivan G. Stassun[1,2], and Robert D. Mathieu[3]
[1] Department of Physics and Astronomy, Vanderbilt University, Nashville, TN 37235, USA
[2] Department of Physics, Fisk University, Nashville, TN 37208, USA
[3] Department of Astronomy, University of Wisconsin–Madison, Madison, WI 53706, USA
Received 2019 November 26; revised 2020 August 26; accepted 2020 August 29; published 2020 October 16

Abstract

We present higher-order multiplicity results for 60 solar-type spectroscopic binaries based on 0.75 μm imaging data taken by the robotic adaptive optics (Robo-AO) system at the Kitt Peak 2.1 m telescope. Our contrast curves show sensitivity up to ∼5 mag at ∼1″ separation; at very small separations, we identify candidate companions from image deviations relative to the point spread function. We find candidate tertiary companions for 62% of our binaries overall, but we find that this fraction is a strong function of the inner binary orbital period; it ranges from ∼47% for $P_{\rm bin} > 30$ days to as high as ∼90% for $P_{\rm bin} \lesssim 5$ days. We similarly find an increasing tertiary companion frequency for shorter-period binaries in a secondary sample of Kepler eclipsing binaries observed by Robo-AO. Using Gaia distances, we estimate an upper limit orbital period for each tertiary candidate and compare the tertiary-to-binary period ratios for systems in the field versus those in star-forming regions. Taken all together, these results provide further evidence for angular momentum transfer from three-body interactions, resulting in tight binaries with tertiaries that widen from pre-main-sequence to field ages.

Unified Astronomy Thesaurus concepts: Binary stars (154); Trinary stars (1714); Dynamical evolution (421)

Supporting material: machine-readable tables

1. Introduction

Although many of the underlying mechanisms and outcomes of the star formation process remain under debate, the prevalence of stellar multiplicity is undisputed, with more than half of all stars having at least one companion. In the past decade, stellar multiplicity studies (e.g., Raghavan et al. 2010; Sana et al. 2014; Tokovinin 2014a; Fuhrmann et al. 2017) have focused on volume-limited samples in distinct spectral-type ranges to achieve unbiased statistical inferences of multiple systems. Others (e.g., Rucinski et al. 2007; Riddle et al. 2015; Hillenbrand et al. 2018) have used high-resolution adaptive optics imaging to identify and characterize new systems.

In particular, high spatial resolution campaigns at longer wavelengths have the ability to maximize detections of faint distant companions. Tokovinin et al. (2006) surveyed 165 solar-type spectroscopic binaries (SBs) and found that virtually all (∼96%) short-period binary systems ($P_{\rm bin} < 3$ days) had tertiary companions.

This seminal finding has motivated a number of follow-up studies to explore the potential effects and evolutionary pathways of binaries in tertiary systems. The dynamics introduced by tertiaries could have significant consequences for the evolution of young stellar objects. For example, in the most recent review of benchmark pre-main-sequence (PMS) eclipsing binaries (EBs), Stassun et al. (2014) found that the properties of those in triple systems constituted the most highly discrepant cases when compared to PMS stellar evolution models, which may be explained if the tertiary inputs significant energy into one or both binary stars during periastron passages (see, e.g., Gómez Maqueo Chew et al. 2019).

More generally, the dominant physical mechanism by which the tertiary influences the creation of tightly bound binaries has not yet been established. Lidov–Kozai cycles with tidal friction (KCTF; Eggleton & Kiseleva-Eggleton 2001) have been hypothesized but require a long dynamical timescale and only operate for certain mutual orbital inclinations. Thus, KCTF is suspected to only be capable of producing a fraction of the total known population of close binaries.

Recent simulations of newborn triple systems (e.g., Reipurth & Mikkola 2012) have found binary orbital hardening occurring early in the systems' evolution, whereby compact triple systems dynamically unfold into wider hierarchical structures. In this scenario, triple systems find themselves in the tight binary–wide tertiary configuration well before evolving onto the main sequence. These findings have been corroborated by recent population synthesis work (e.g., Moe & Kratter 2018), which found that ∼60% of close binaries form in this manner, with additional energy dissipation arising from primordial gas–disk interactions in the binary.

Making progress in determining the respective rates of these different mechanisms requires a greater number of binary-star systems with well-known periods, distances, and ages and for which the presence of a tertiary companion is well established. In addition, the fundamental result of an increased tertiary occurrence among the tightest binaries (Tokovinin et al. 2006) should ideally be reproduced with independent samples, given its importance in motivating and constraining these questions.

In this paper, we seek to test the reproducibility of the cornerstone result of Tokovinin et al. (2006) and explore the evidence of potential evolutionary pathways for triple systems. In Section 2, we describe our sample of observed binaries and list some of their fundamental physical properties. We also describe the source and nature of our data, along with data reduction and processing procedures. In Section 3, we describe our search for additional companions to our sample using published catalogs and with Gaia DR2, in some cases offering additional confirmation of our robotic adaptive optics (Robo-AO) multiplicity identifications. In Section 4, we report the results of our Robo-AO SB multiplicity survey and compare with complementary Robo-AO observations of Kepler EBs. In Section 5, we discuss the implications of our results on current

Table 1
Robo-AO Non-SB Observations

Name	R.A. (deg.)	Decl. (deg.)	V (mag)	Strehl Ratio (%)	Multiplicity Flag[a]
2MASS J05130342+2423489	78.264217899	24.396841655	6.707	2.06	T
2MASS J08140761+3145095[b]	123.531723248	31.752562931	12.44	6.52	
2MASS J08145689+3208572	123.736957886	32.149168567	8.3	4.51	B
2MASS J09303285+2735099	142.636911616	27.585936424	10.722	3.56	N
2MASS J10404394+2348227	160.18296347	23.806274661	10.382	2.3	N
2MASS J11040722+4415409	166.029847747	44.261378235	9.685	3.66	B
2MASS J11464736+3424349	176.69737612	34.409630054	10.378	2.14	N
2MASS J13312997+3813115	202.874932285	38.219833319	10.839	2.86	N
2MASS J13334365+3754543	203.431735917	37.915035417	10.219	1.96	N
2MASS J13392768+2726135[b]	204.864597905	27.437240111	11.777	6.72	
2MASS J15055682+2216202	226.486763946	22.27226675	8.71	3.36	B
2MASS J15120615+6826579	228.025462449	68.449601426	9.621	1.68	N
2MASS J16385624+3652029	249.734407561	36.867416544	10.311	2.72	N
2MASS J17205010+4223016	260.208784546	42.38376309	10.75	3.87	B
2MASS J19303059+3751364	292.627494341	37.860165321	10.688	4.86	B
2MASS J19344300+4651099	293.6792058	46.852733735	7.768	1.26	N

Notes.
[a] Multiplicity flag: B = candidate binary, T = candidate triple, N = no companion detected.
[b] Faint systems that were not reduced properly (see Section 2.1; no companion information could be deduced from Robo-AO imaging).
(This table is available in machine-readable form.)

star formation and binary evolution theory. Finally, in Section 6, we conclude with a brief summary of our findings.

2. Data and Methods

2.1. SB Star Samples Used

The goals of this study include examining multiplicity fractions as a function of inner binary period and comparing the derived properties of our identified candidate tertiaries with known multiples from the literature. Therefore, our Robo-AO target list required a large sample of SBs with known orbital periods and distances. To this end, we use the Troup et al. (2016) sample of main-sequence Apache Point Observatory Galactic Evolution Experiment (APOGEE) stars identified with stellar and substellar companions, which includes 178 systems within 1 kpc. In addition, we also include the Torres et al. (2010) sample of benchmark EBs (EBs that are also SBs). These 94 systems have known orbital periods and distances (Stassun & Torres 2016), as well as component masses and radii derived to an accuracy of 1%–3%.

These two samples constitute the master list of SBs in our Robo-AO survey, of which we have observed 33 EBs from the Torres et al. (2010) sample and 43 targets from the Troup et al. (2016) sample, with the orbital periods of the combined sample spanning the range 0.3–1880 days. Although all 43 Troup sources are radial velocity variable, we verify a clean sample of SBs by requiring the derived minimum mass of the companion to be greater than that of a brown dwarf ($0.013M_{\odot}$). We also conservatively require the significance of the radial velocity variations in sigma units to be greater than 10. This identifies 27 Troup et al. (2016) SBs (thus, 33 + 27 = 60 SBs in total) for our sample. We do not consider the remaining 16 Troup et al. (2016) stars in our analysis in Sections 3 or 4, but for the benefit of future studies, we report any companions that we identified in our Robo-AO imaging in Table 1. All of the targets in our sample have parallaxes reported in the Gaia second data release (DR2) with distances in the range 40–2200 pc. Graphical summaries of some basic parameters for our Robo-AO SB sample are displayed in Figure 1. Their properties and identifications are listed in Table 2.

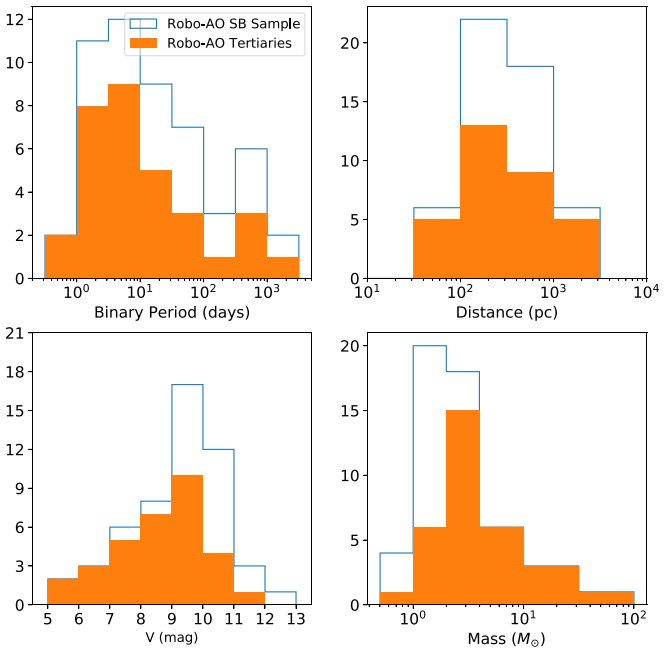

Figure 1. Representative histograms of stellar properties for the Robo-AO SB sample (open) and the subset with identified candidate tertiary companions (filled). We note that the mass histograms refer to binary mass, except for our Troup et al. (2016) sources, which only have known mass values for the primary. The bias against detection of very low mass companions (lower right panel) is a reflection of the sensitivity limit of our data for faint sources (lower left panel).

For an independent test sample, we also made use of the published Robo-AO observations of Kepler EBs from Law et al. (2014), originally drawn from the master sample of Kepler objects of interest (KOIs). To enable a direct comparison with our Robo-AO sample, we trim the initial sample of 1065 KOI EBs as follows. To remove potential EB false positives, we required a minimum primary eclipse depth

Table 2
Robo-AO SB Sample

Name	R.A. (deg)	Decl. (deg)	P_{bin} (days)	V (mag)	Multiplicity Flag[a]	Sample ID[b]
V432 Aur	84.38524	37.08689	3.082	8.05	T	Stassun & Torres—EB
WW Aur	98.11313	32.45482	2.525	5.82	T	Stassun & Torres—EB
HS Aur	102.82702	47.67335	9.815	10.05	B	Stassun & Torres—EB
HD 71636	127.48465	37.07095	5.013	7.90	U	Stassun & Torres—EB
KX Cnc	130.69238	31.86242	31.22	7.19	T	Stassun & Torres—EB
2MASS J10352794+2512348	158.86626	25.20971	25.09	9.73	B	Troup—SB
2MASS J11452973+0159347	176.3738	1.99299	1033.875	9.96	B	Troup—SB

Notes.
[a] Multiplicity flag: B = binary, T = triple, U = undetermined (Section 2.2).
[b] Sample ID: Stassun & Torres—EB = EBs from Stassun & Torres (2016); Troup—SB = SBs from Troup et al. (2016).
(This table is available in its entirety in machine-readable form.)

of 1 mmag, as fit by the Kepler EB pipeline's `polyfit` algorithm (Prša et al. 2008). Similarly, we also required all systems to have a successful "morphology" classification (between zero and 1), as output by the local linear embedding (LLE) of the Kepler EB pipeline (Matijevič et al. 2012). We excluded all targets fainter than the faint limit of our sample ($V < 12.5$) by converting their Kepler magnitudes to V via the published Kepler color–temperature relation. This also requires the EBs to have nominal effective temperatures listed in the Kepler Input Catalog. This leaves a remaining sample of 109 KOI EBs.

Of these 109, 52 have Robo-AO observations, of which 22 have clear determinations of the presence or absence of a companion (Table 3). These identifications correspond to multiple Robo-AO KOI survey efforts taken at the Palomar 1.5 m telescope, including Law et al. (2014), Baranec et al. (2016), and Ziegler et al. (2017, 2018a, 2018b).

Table 3
Robo-AO KOI EB Sample

KOI	R.A. (deg)	Decl. (deg)	P_{bin} (days)	V (mag)	Multiplicity Flag[a]
5774	283.86634	47.22828	2.4275	10.834	T
5993	285.14501	39.18703	4.2647	13.0	T
971	286.01929	48.86677	0.5331	7.642	B
6109	287.83336	39.22124	22.9135	11.911	T
1728	288.97163	44.62465	12.7319	12.069	B
2758	289.74253	39.26713	253.3623	12.168	B
1661	290.73807	39.91969	1.8955	11.601	T

Note.
[a] Multiplicity flag: B = binary, T = triple.
(This table is available in its entirety in machine-readable form.)

2.2. Robo-AO Imaging

Robo-AO is an autonomous laser adaptive optics system stationed at the Kitt Peak 2.1 m telescope from 2015 November to 2018 June. Robo-AO has a field size of 36″ on a side with a pixel scale of 35.1 mas pixel^{-1} (Jensen-Clem et al. 2017). High spatial resolution images of the target stars were taken between 2017 November and 2018 June. We observed 76 unique targets in the i' bandpass (6731–8726 Å) with 90 s exposures. Over the 90 s exposure, about 773 individual frames are generated. Target images were initially processed with the Robo-AO "bright star" pipeline as described in Law et al. (2014).

While this pipeline was appropriate for the majority of our Robo-AO SB images, we note five faint SB systems (2MASS IDs J07381910, J16515260, J19301035, J19305116, and J19412976) that were not properly reduced. As noted in Jensen-Clem et al. (2017), the images in these cases failed to correctly center the point-spread function (PSF), leading to a single noticeably bright pixel in the center of the image. We remove these targets from the sample to avoid biasing our multiplicity analysis in Section 4, leaving 55 SBs. To maximize our detection of tertiaries at small angular separations, the images were further processed by the "high-contrast imaging" pipeline described in Jensen-Clem et al. (2017).

This pipeline first applies a high-pass filter on a 3.″5 frame windowed on the star of interest to lessen the contribution from the stellar halo. A synthetic PSF is then subtracted, generated via Karhunen–Loève image processing (KLIP, a principal component analysis algorithm that whitens correlated speckle noise; Soummer et al. 2012). A representative sample of PSF diversity is achieved using a reference library of several thousand 3.″5 square high-pass-filtered frames that have been visually vetted to reject fields with more than one point source. This technique of reference star differential imaging (RDI; Lafrenière et al. 2009) results in the final PSF-subtracted image, from which we make our multiplicity determinations.

Measurement of multiple-star systems' position angles (PAs) and separations also require a precise astrometric solution for the optical instrument. Nightly observations of densely populated globular clusters are used to establish and update this solution as described in Section 6 of Jensen-Clem et al. (2017). After each science target is fully reduced, the pipeline also produces a 5σ contrast curve by simulating companions and properly correcting for algorithmic throughput losses using the vortex image processing (VIP) package (Gomez Gonzalez et al. 2017). Examples of our Robo-AO images pre- and postprocessing, along with their corresponding contrast curves, are shown in Figure 2.

The expected Robo-AO error budget and performance is summarized in Table 2 of Jensen-Clem et al. (2017). At our observed Strehl ratios of a few percent, we expect a delivered FWHM of ∼0.″15. The majority of our SB sample has unambiguous nondetections or else distortions suggestive of a tertiary companion upon visual inspection of their PSF-subtracted images. We assign a multiplicity flag of "T," for the cases with clear image distortions, or "B" for cases of undetected companions. In a small number of cases, we observe residuals that weakly imply a quadruple but are suspected to be artifacts from the PSF-subtraction process. We assign these cases a multiplicity flag of "T(Q?)" in Figures 9–11 in the Appendix.

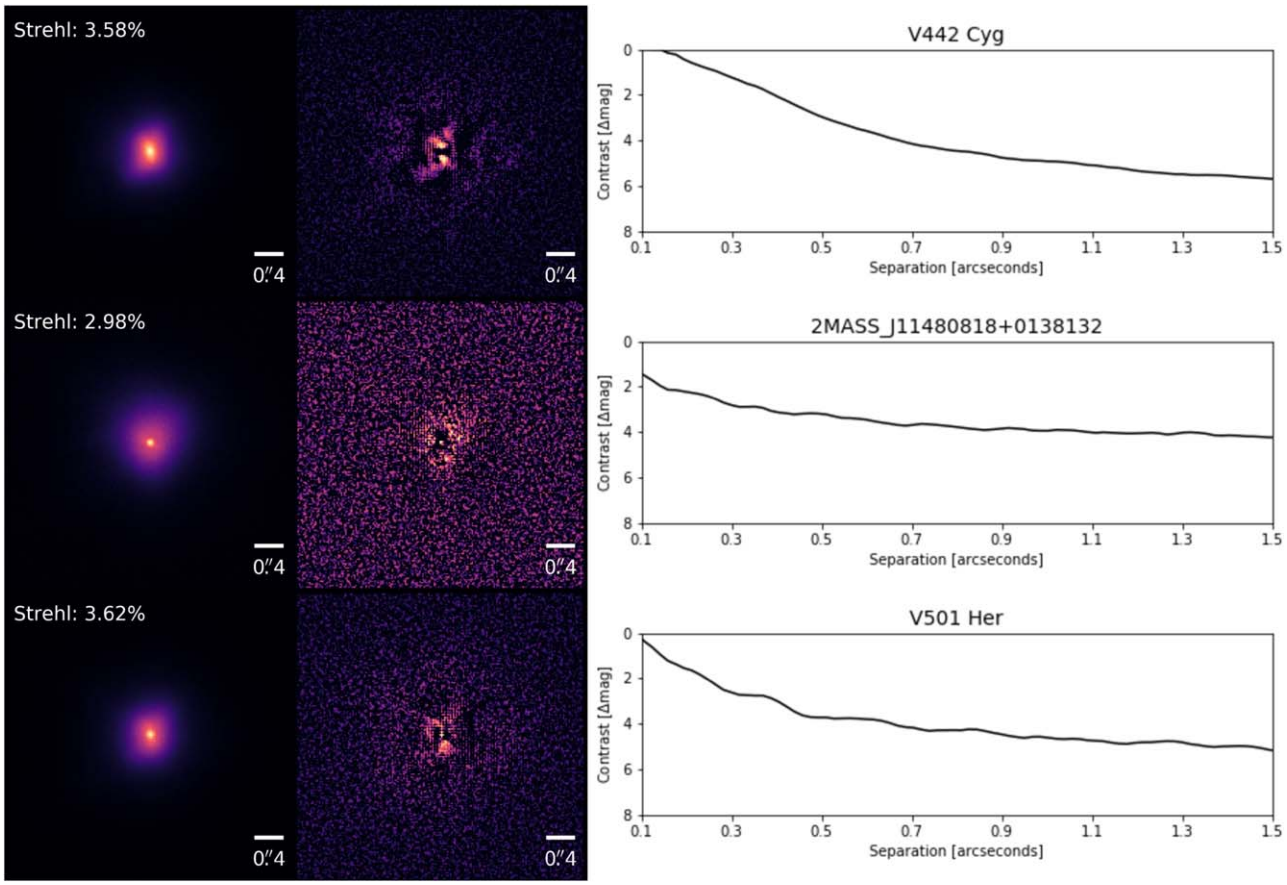

Figure 2. Top panels: Robo-AO image (left), PSF-subtracted image (middle), and contrast curve (right) of V442 Cyg; residuals reveal distortion in the pre-subtracted image that suggests a tertiary companion to the unresolved SB. Middle panels: Robo-AO image, PSF-subtracted image, and contrast curve of 2MASS J11480818 +0138132; residuals clearly do not suggest a tertiary companion. Bottom panels: Robo-AO image, PSF-subtracted image, and contrast curve of V501 Her; residuals indicate an unclear case.

Lastly, three cases have difficult-to-interpret residuals for which we are unable to determine identifications (Figure 2, lower right panel) and are thus assigned a multiplicity flag of "U." Our analysis in Section 4 excludes all unclear cases, resulting in a remaining sample of 52 SBs.

To be clear, we do not resolve individual components for the majority of our Robo-AO observations (Figure 9–11 in the Appendix). Many of the triples suggested in the PSF-subtracted images are the result of clear elongation compared to the point source–like observations of SBs with no detected companions. While the residuals from this process do not allow us to unambiguously identify the presence of a companion, we use them to flag candidates and then further vet the sample with Gaia astrometry and with previous observations (Section 3).

We note the image residuals cannot be used to reliably measure flux contrasts; for each identified candidate tertiary, we only measure an upper limit to its angular separation and a PA by measuring the positions of the two peaks in the PSF-subtracted images, representing the angular scale of the image distortion (i.e., the combined effect of the central unresolved SB and the putative tertiary companion), carefully accounting for the slight difference in x and y pixel scales (noted in the Appendix of Jensen-Clem et al. 2017).

While the distribution of PAs (Figure 3) is statistically consistent with a uniform distribution as expected, there may be a slight preference for PAs near 180°/360° that could be

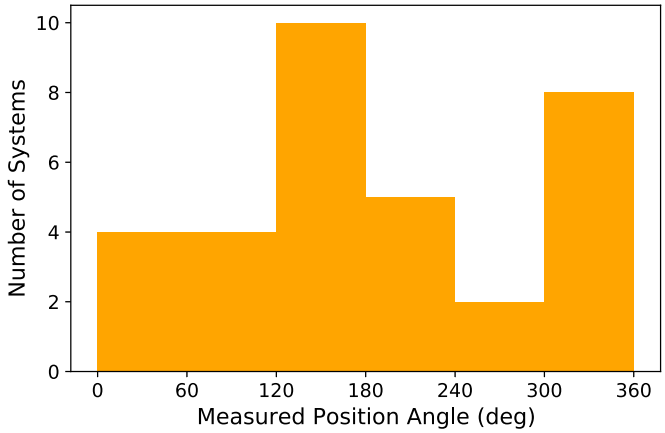

Figure 3. Distribution of measured position angles from Robo-AO PSF-subtracted image residuals.

nonphysical; these systems would benefit from follow-up observation (but see also Section 3). The angular separations are then translated into physical upper limit projected separations using the Gaia DR2 distance to each system. We note that the masses for each target have been sourced from the literature and correspond to the binary mass, except for our Troup et al. (2016) sources, which only have known mass values for the primary. These masses are used to derive a rough upper limit estimate of the tertiary period. We report its

Table 4
Robo-AO and Gaia Identified Candidate Tertiaries

Name	P_{bin} (days)	Sep. (arcsec)[a]	Dist. (pc)	Proj. Sep. (au)[a]	Mass ($M_{\odot}$)[b]	~log (P_3) (yr)[a]	GOF_AL[c]	D[d]
V432 Aur	3.082	0.12	127.1	15.6	2.3	1.2	5.45	0.0
WW Aur[e]	2.525	0.13	90.9	12.2	3.8	0.9	29.27	32.69
KX Cnc	31.22	0.12	49.3	6.1	2.3	0.5	11.84	0.0
2MASS J11480818+0138132[f]	400.82	119.1	235.0	27988.1	1.1	6.2	64.57	223.42
2MASS J12260547+2644385	300.056	0.22	127.4	27.7	0.8	1.8	33.07	80.09
BH Vir	0.817	0.19	149.3	28.1	2.2	1.5	7.75	0.0
AD Boo[e]	2.069	0.25	195.4	49.6	2.6	1.9	25.38	13.91
2MASS J15044648+2224548	45.595	0.19	67.2	12.9	1.2	1.2	22.45	14.48
2MASS J15212898+6722473	767.137	0.20	255.3	51.6	1.2	2.1	15.69	10.56
RT CrB	5.117	0.21	401.1	85.8	2.7	2.2	8.9	0.0
V335 Ser[e]	3.45	0.22	202.3	43.9	4.1	1.7	17.46	3.97
2MASS J16063131+2253008	1316.38	0.16	86.2	13.6	1.2	1.2	40.87	45.54
2MASS J16100946+2312212[e]	75.887	0.26	437.1	114.5	1.2	2.6	20.31	3.71
WZ Oph	4.184	0.18	156.9	28.7	2.4	1.5	9.31	0.0
V2365 Oph[e]	4.866	0.20	254.4	51.1	3.0	1.9	15.29	4.27
V2368 Oph	38.327	0.18	217.6	38.1	4.9	1.6	20.24	10.79
LV Her	18.436	0.25	374.2	94.3	2.4	2.3	11.3	0.0
V624 Her[e]	3.895	0.18	140.6	25.9	4.2	1.4	28.95	21.52
KIC 8410637	408.324	0.16	1266.7	200.1	2.8	2.8	13.55	0.0
DI Her[e]	10.55	0.16	650.5	103.4	9.7	2.1	24.51	7.28
FL Lyr	2.178	0.20	135.0	26.5	2.2	1.5	10.11	0.0
V885 Cyg[e]	1.695	0.21	964.0	206.3	4.2	2.7	21.82	5.05
KIC 3858884	25.952	0.19	552.8	106.7	3.7	2.3	13.12	0.0
V380 Cyg[e]	12.426	0.14	1061.9	150.8	18.4	2.2	66.94	103.34
V453 Cyg	3.89	0.17	1518.0	255.0	25.0	2.5	10.54	0.0
V478 Cyg	2.881	0.18	2222.8	406.8	30.4	2.7	8.21	0.0
MY Cyg	4.005	0.17	250.5	41.8	3.6	1.7	9.17	0.0
V442 Cyg	2.386	0.19	340.5	64.3	3.0	2.0	7.68	0.0
Y Cyg[e]	2.996	0.16	1735.2	277.6	35.5	2.4	22.83	7.64
CG Cyg	0.631	0.22	97.5	21.5	1.8	1.4	8.94	0.0
V364 Lac	7.352	0.15	410.5	61.2	4.6	1.9	14.33	0.0
BK Peg[f]	5.49	104.3	318.6	33257.6	2.7	6.1	11.56	0.0

Notes.
[a] We note that the reported quantities in these columns are upper limits.
[b] For Stassun & Torres SBs, masses are sourced from the detached EB catalog (DEBCat; Southworth 2015).
[c] Gaia astrometric goodness of fit in the along-scan direction.
[d] Gaia significance of the astrometric excess noise.
[e] Multiple status astrometrically confirmed by Gaia (Section 3.2).
[f] Wide tertiary companion identified by Gaia CPM analysis (Section 3.1).

(This table is available in machine-readable form.)

logarithm, along with our measured angular and projected separations for all of our multiple systems, in Table 4. We note that our period estimates, however, can significantly vary from the true period in cases where the projected separation is much different than the true semimajor axis of the system.

The resolution and sensitivity limits of our Robo-AO observations hinder our ability to detect long-period ($P_3 \gtrsim 10^4$ yr) tertiaries. The $3\farcs5$ frame centered on each of our sources corresponds to a maximum detectable angular separation of $1\farcs75$. For a typical tertiary in our sample, this corresponds to a tertiary period of ~9200 yr. Thus, very long period ($P_3 \gtrsim 10^4$ yr) tertiaries generally do not fall within our Robo-AO field of view.

3. Catalog Search for Additional Companions

As the most sensitive probe of parallaxes and proper motions, Gaia (Gaia Collaboration et al. 2016, 2018) provides a powerful opportunity to search more comprehensively for additional companions to our Robo-AO SB sample. Resolved common proper-motion (CPM) companion matches have the ability to corroborate, or in some cases refine, our prior multiplicity determinations. Additionally, astrometric-quality information on unresolved companions can similarly serve to confirm Robo-AO-identified multiples. As a final companion check, we also query the Washington Double Star (WDS) catalog for prior multiplicity information on our Robo-AO targets.

3.1. Gaia CPM Candidates

We begin by crossmatching our Robo-AO SBs with the Gaia DR2 catalog to obtain both parallax and proper-motion information for each target. We then query Gaia DR2 to list all targets found within a $5'$ aperture centered on each Robo-AO binary. The aperture size chosen searches for any wide companions outside of our $3\farcs5$ Robo-AO field of view while minimizing those with separations that are unlikely to be bound. For both this larger sample and our Robo-AO–Gaia crossmatch, we apply the suggested corrections to the published Gaia DR2 magnitudes following Evans et al. (2018) and Maíz Apellániz & Weiler (2018),

depending on the magnitude range considered. For the brighter ($G < 11.5$) stars in both samples, we also apply a proper-motion correction due to the inertial spin of the Gaia DR2 proper-motion system (Lindegren et al. 2018).

Our wide search returns 49,343 sources, 6810 of which do not have parallax or proper-motion information. With the remaining 42,533 sources, we follow a similar procedure to the Gaia companion candidate cuts chosen by Jiménez-Esteban et al. (2019) to find wide comoving binaries. In our case, we choose more lenient fractional error cuts on parallax (20%) and proper motion (50%) to maximize our chances of identifying fainter companions while still ensuring reasonably high-quality measurements. This vetting reduces the total number of candidate companions to 5332.

To check for CPM companions that are likely to be physically associated, we then compare the parallax and proper-motion information on these candidates with their corresponding Robo-AO counterpart. We require their respective parallax and proper-motion measurements to agree within 2.5σ, with σ being the larger error of the two. For the remaining 10 candidates, we estimate their projected separations, with distances derived from the error-weighted arithmetic mean parallax of each pair. Again, we note that these estimates can vary significantly from the true semimajor axis of the orbit. As a final requirement, we set a generous separation threshold of 50,000 au to exclude pairs that are most likely not physically bound while recognizing the approximate nature of our derivations.

The result is the identification of three CPM companion candidates. We report a faint ($G \sim 18.9$) companion to RT CrB at an angular separation of $9\farcs5$. We change its multiplicity designations from triple candidate to quadruple candidate and make a note of its nonhierarchical ($2 + 1 + 1$) configuration. We also report a faint ($G \sim 18.9$) companion to BK Peg at an angular separation of $104\farcs4$ and a ($G \sim 11$) companion to 2MASS J11480818+0138132 at an angular separation of $119\farcs1$. We change their multiplicity designations from binary to triple.

Lastly, we return to the subsample of 7108 sources that Gaia does not record parallax or proper-motion information for. Although these sources cannot be vetted for association, we check for those that have separations from their Robo-AO counterpart near Gaia's resolution limit of $1''$. We find one match to 2MASS J12260547+2644385, a confirmation of the wide ($\sim 1''$) triple companion confirmed in our Robo-AO imaging. Considering the other Robo-AO system with a relatively wider companion in the Robo-AO field of view, we find the ($\sim 1''$) triple companion for CG Cyg is not detected by Gaia. However, considering the proximity to Gaia's resolution limit, as well as the rarity of chance alignments at these separations, we choose to leave its multiplicity designation unchanged.

3.2. Gaia Astrometric Candidates

Significant deviations from Gaia's astrometric fit, manifesting as large values of the astrometric goodness of fit in the along-scan direction (GOF_AL) and the significance of the astrometric excess noise (D), hint at the presence of unresolved companions. In particular, Evans (2018) found a cutoff of GOF_AL > 20 and $D > 5$ to best separate confirmed binaries from confirmed singles. To confirm the source of the astrometric noise, we explore its dependence as a function of inner binary separation using the slightly relaxed criterion of GOF_AL > 15 and $D > 3$.

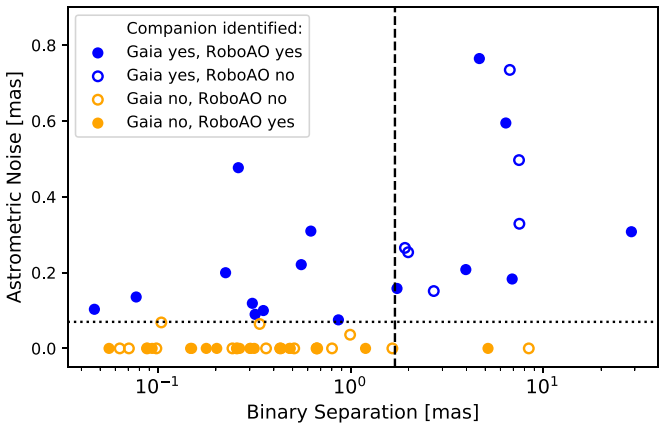

Figure 4. Gaia recorded astrometric noise for our Robo-AO SBs as a function of inner binary separation. Systems that (do not) pass our Gaia astrometric criterion (GOF_AL > 15 and $D > 3$) are shown in blue (orange). Filled (open) dots correspond to cases where our Robo-AO imaging (did not) identified a candidate companion within $3.5''$. The dotted line denotes the minimum astrometric noise observed for systems that pass our astrometric criterion. The dashed line separates our tighter (left) and wider (right) Robo-AO SBs.

As we show in Figure 4, Gaia does not register significant astrometric noise (threshold marked by the dotted line) for the majority of our Robo-AO SBs, which typically have inner binary separations $\lesssim$1.5 mas (left of dashed line). For those that do register astrometric noise in this regime, we find that all (10) systems also have a candidate companion identified in our Robo-AO imaging. We conclude that systems whose central SBs are tighter than $\sim$1.5 mas are not noticed as multiples by Gaia unless they also possess a wider tertiary.

In contrast, we find that the vast majority (12/14) of our wider SBs ($\gtrsim$1.5 mas; right of dashed line) register significant astrometric noise values (above dotted line), even if they do not possess an identified tertiary companion. In this regime, Gaia is likely detecting the photocenter motion of the relatively wide SBs, regardless of whether there is a wider tertiary.

A similar analysis for our Robo-AO KOI EB sample also confirms our tertiary designations. The sole exception is KOI 6016, for which Gaia identifies significantly high values of GOF_AL $= 166$ and $D = 2095$. Assuming a total binary mass of 2 $M_\odot$, we estimate the angular separation of the EB (0.677 mas) to be much smaller than its measured astrometric excess noise (2.38 mas); thus, we argue that its source is an unresolved tertiary companion. We change its designation from binary to tertiary.

3.3. WDS Catalog Comparison

In this section, we carefully compare our observations to those listed in the WDS catalog. We find that eight of our Robo-AO SB targets have entries and describe them individually below.

2MASS J11480818+0138132—The most recent companion identification listed in WDS entry 11482+0136 refers to observations in 2015 by the Garraf Astronomical Observatory (OAG). Its CPM wide pair (WP) survey identified[4] a $V \sim 11.1$

[4] The OAG CPMWP catalog can be found at https://www.oagarraf.net/Comunicacions/OAG%20CPM/GWP%20CATALOG%20EQUATORIAL%20ZONE%202016_ASCII__1.0.txt.

companion at a separation of 119.″1 with a PA of 334°. While this target is outside of the field of view of our Robo-AO imaging, our Gaia CPM analysis (see Section 3.1) also identifies this wide companion.

2MASS J12260547+2644385—WDS entry 12261+2645 refers to a singular speckle-interferometric observation that identified a $V \sim 9.7$ companion at a separation of 1.″1 with a PA of 167° (ASCC No. 684901 in Guerrero et al. 2015). Our Robo-AO observations find 2MASS J12260547+2644385 to be a candidate triple, with an upper limit separation of 1.″11 and a PA of 346°. Given our convention of measuring PA with respect to the SB (346°–180° = 166°), we find these results to be in agreement and confirm this companion.

2MASS J16063131+2253008—The most recent companion identification listed in WDS entry 16065+2253 refers to Pan-STARRS observations from 2015, as detailed by Deacon et al. (2014). They reported a companion separation of 35.″5 at a PA of 22°. The proposed source, 2MASS J16063229+2253337, is resolved by Gaia but faint ($G \sim 19.3$). Gaia reports a parallax, R.A. proper motion, and decl. proper motion of 11.734 ± 0.418 mas, -84.088 ± 0.538 mas yr^{-1}, and 90.03 ± 0.571 mas yr^{-1}. In comparison, Gaia reports 11.601 ± 0.075 mas, -88.263 ± 0.105 mas yr^{-1}, and 72.873 ± 0.124 mas yr^{-1} for 2MASS J16063131+2253008. Given in particular the difference in decl. proper motion, our Gaia CPM analysis does not find this pair to be associated.

2MASS J16074884+2305299—The most recent companion identification listed in WDS entry 16078+2306 refers to a 2004 observation (Alam et al. 2015) that identified a $V \sim 13.3$ companion at a separation of 12.″2 with a PA of 81°. A source at this separation does not fall into our Robo-AO field of view. Gaia resolves one other source within 15″, Gaia DR2 1206535963616734976, and reports a parallax, R.A. proper motion, and decl. proper motion of 0.735 ± 0.02 mas, 3.58 ± 0.03 mas yr^{-1}, and -9.18 ± 0.03 mas yr^{-1}. In comparison, Gaia reports 2.04 ± 0.036 mas, -3.48 ± 0.04 mas yr^{-1}, and -9.38 ± 0.05 mas yr^{-1} for 2MASS J16063131+2253008. These sources are clearly not physically associated.

V2368 Oph—WDS entry 17162+0211 refers to a singular 1985 speckle-interferometric observation from the Center for High Angular Resolution Astronomy (CHARA; McAlister et al. 1987). They reported a separation of 0.″136 at a PA of 69°. As detailed in the auxiliary WDS notes, the WDS entry was recalled after repeated attempts at confirmation by McAlister but later restored. While the most recent effort to confirm this companion (Roberts & Mason 2018) was unsuccessful, our Robo-AO imaging suggests a candidate companion at an upper limit separation of 0.″175 at a PA of 68°. Given the close agreement in separation and PA, we tentatively confirm this candidate companion but encourage continued monitoring of this clearly complex case.

V624 Her—The most recent companion identification listed in WDS entry 17443+1425 refers to a 2015 Gaia DR1 observation (Knapp & Nanson 2018) that identified a $V \sim 11.75$ companion at a separation of 40″ with a PA of 151°. Gaia DR2 reports a parallax, R.A. proper motion, and decl. proper motion of 7.1119 ± 0.0628 mas, -2.271 ± 0.098 mas yr^{-1}, and 15.134 ± 0.096 mas yr^{-1} for V624 Her. In comparison, Gaia DR2 reports 0.7206 ± 0.0457 mas, -0.446 ± 0.074 mas yr^{-1}, and -3.962 ± 0.070 mas yr^{-1} for WDS 17443+1425B. These sources are clearly not physically associated.

V478 Cyg—The most recent companion identification listed in WDS entry 20196+3820 refers to a 2015 listing in the Webb Deep-Sky Society's Double Star Section Circulars (DSSC).[5] The listing, a 2006 observation from UKIDSS DR6, identifies a $V \sim 14.5$ companion at a separation of 3.″61 with a PA of 258°. A source at this separation does not fall into our Robo-AO field of view. Gaia resolves one other source within 5″ of V478 Cyg but shows the pair to have discrepant parallaxes. We opt to retain our original identification.

CG Cyg—The most recent companion identification listed in WDS entry 20582+3511 refers to two speckle-interferometric observations in 2014 that identified a $V \sim 12$ companion at a separation of 1.″1 with a PA of 310° (Horch et al. 2015). Our Robo-AO observations find CG Cyg to be a triple, with a tertiary companion at an upper limit separation of 1.″16 and a PA of 313°. Given the close agreement in separation and RA, we confirm this companion.

Given the faintness of the two wide companions we identified in Section 3.1 ($G \sim 19$), it is not surprising that the WDS catalog does not list entries for RT Crb or BK Peg. Similarly, the remaining 43 Robo-AO SBs do not have entries in the WDS catalog, likely a consequence of the difficulty of finding visual companions at the proximity of the (upper limit) separations of Robo-AO-identified candidate companions ($\leqslant$0.″25).

4. Results

To summarize our analysis in Sections 2–3, out of our initial sample of 55 SBs, we obtain Robo-AO determinations in 52 cases. After our catalog search for additional CPM and astrometric candidate companions, we report a final tally of 20 binaries, 31 candidate triples, and one candidate quadruple system.

We begin by exploring the dependence of tertiary companion frequency on inner SB period for our Robo-AO SBs. Our 52 systems are sorted into SB period bins, with bin edges of 0, 3, 6, and 30 days (Figure 5, orange). Systems with periods greater than 30 days are grouped together (rightmost point). We find a trend of increasing incidence of tertiary companions toward shorter-period SBs (orange points), with 90% of 3 day $< P_{\rm bin} <$ 6 day SBs having a tertiary companion compared to ∼47% of the longest-period ($P_{\rm bin} >$ 30 day) SBs. In the shortest-period bin ($P_{\rm bin} <$ 3 days), we find a slightly decreased fraction of 75% relative to the next bin (3 days $< P_{\rm bin} <$ 6 days). We report the resultant tertiary fraction we derive for each period bin with its error in Table 5.

To compare with the canonical trend originally reported by Tokovinin et al. (2006), in Figure 5 we represent the Tokovinin et al. (2006) tertiary fractions with a simple exponential (note that this is not intended to represent a physical model). The tertiary fractions that we observe as a function of inner binary period are broadly consistent with the Tokovinin et al. (2006) result. We find that this trend also extends to binary periods of $P_{\rm bin} >$ 30 days, which are even longer than those considered by Tokovinin et al. (2006).

Next, as outlined in Section 2.1, we use the KOI EBs observed by Robo-AO as an additional, independent test sample of this trend. These systems had their PSF-subtracted images analyzed to look for stars within 4″ of the central target (references in Section 2.1). Our Gaia analysis (Section 3.1)

[5] The DSSC catalog can be found at https://www.webbdeepsky.com/dssc/dssc23.pdf.

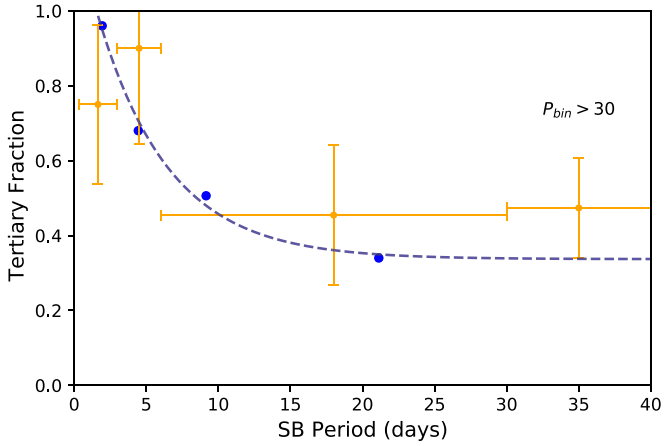

Figure 5. Fraction of SB systems with a candidate tertiary companion as a function of binary period (orange). The final bin represents all SBs with $P_{\rm bin} > 30$ days. In blue, we overplot the tertiary fractions found in Tokovinin et al. (2006), fit with a decaying exponential. Individual error bars correspond to the adjusted Poisson error for a multinomial distribution.

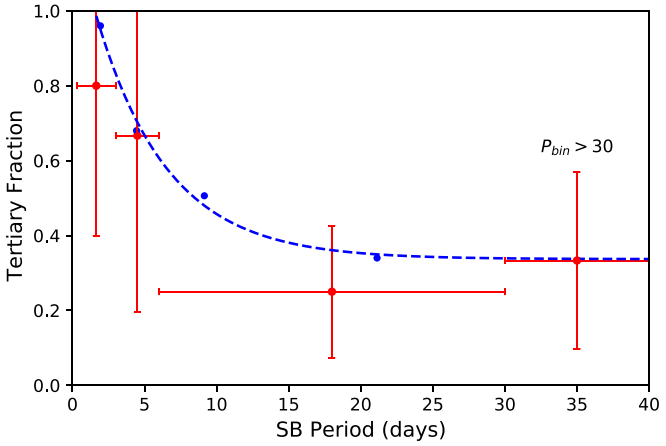

Figure 6. Same as Figure 5 but for KOI EBs observed by Robo-AO (red). The final bin represents all SBs with $P_{\rm bin} > 30$ days.

Table 5
Derived Tertiary Fractions

Period Bin	N	f
Robo-AO SBs		
$P_1 < 3$	12	0.75 ± 0.21
$3 < P_1 < 6$	10	0.9 ± 0.25
$6 < P_1 < 30$	11	0.45 ± 0.19
$P_1 > 30$	19	0.47 ± 0.14
Robo-AO KOI EBs		
$P_1 < 3$	5	0.96 ± 0.4
$3 < P_1 < 6$	3	0.68 ± 0.47
$6 < P_1 < 30$	8	0.51 ± 0.18
$P_1 > 30$	6	0.34 ± 0.24

rules out the wider ($\gtrsim$2″–3″) identified candidate companions. Candidate companions within $\sim$1″ of the targets are considered to be likely physically associated. The resulting tertiary fractions as a function of SB period are shown in Figure 6 and again reported with errors in Table 5.

Although there are only 10 KOI tertiaries among the SBs with $P_{\rm bin} < 30$ days, we find general agreement between our Robo-AO results (Figure 5) and the KOI EB sample (Figure 6). We again find a systematically higher fraction of tertiary companions with shorter-period SBs, with both trends clearly consistent with the findings of Tokovinin et al. (2006). We again note that this trend also seems to extend to binary periods of $P_{\rm bin} > 30$ days.

5. Discussion

5.1. Tertiary-to-binary Orbital Period Ratios

The increasing number of known multiples with well-defined orbital periods has led to a thorough probing of the distribution of tertiary orbital period as a function of inner binary period. In Figure 7, the large sample of known triples from the updated Multiple Star Catalog (MSC; Tokovinin 2018; gray plus signs) and the smaller sample of triples from the volume-limited Raghavan et al. (2010) sample (black plus signs) clearly

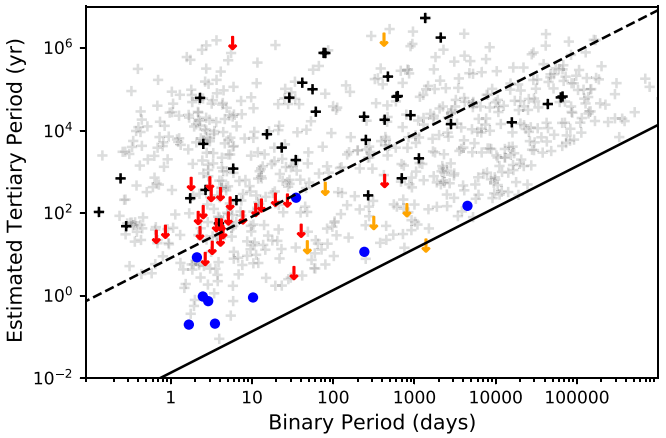

Figure 7. Estimated tertiary periods as a function of inner binary period. Identified Robo-AO candidate triples are marked as red (Torres et al. 2010) and orange (Troup et al. 2016) arrows, given that our estimates are upper limits. For comparison, we plot the updated MSC triples (Tokovinin 2018) as gray plus signs while overplotting the triples from the volume-limited Raghavan et al. (2010) sample as black plus signs. For reference, the dashed line represents $P_3 = 10^{3.5}P_1$. The dynamical stability limit for triples ($P_3 = 4.7P_1$) is shown by the solid line. Known PMS ($\lesssim$30 Myr) triples are shown in blue.

indicate the wide range of permitted tertiary–binary period ratios. However, as noted in both Tokovinin (2014a) and Tokovinin (2018), the rarity of systems with small period ratios (<10), and in particular short tertiary periods ($P_3 < 10$ yr), is evident from the lack of points along the dynamical stability limit $P_3 = 4.7P_1$ (solid line; Mardling & Aarseth 2001) in the lower left corner.

In an effort to explore a potential correlation with age, we refer to the benchmark PMS EB sample (Stassun et al. 2014), in which seven of the 13 are identified with or have evidence of a tertiary companion. Three of these systems (RS Cha, TY CrA, and MML 53; Corporon et al. 1996; Woollands et al. 2013; Gómez Maqueo Chew et al. 2019) have tertiaries with orbital solutions; their ages range from 3 to 15 Myr. A literature search for additional PMS tertiaries also reveals orbital solutions for V1200 Cen (Coronado et al. 2015), GW Ori (Czekala et al. 2017), TWA 3A (Kellogg et al. 2017), V807 Tau (Schaefer et al. 2012), and TIC 167692429 and TIC 220397947 (Borkovits et al. 2020).

The tendency for these PMS systems to lie at low tertiary–binary period ratios is evident in Figure 7. To probe the

potential significance of this apparent difference relative to the older field population, we perform a two-dimensional, two-sided Kolmogorov–Smirnov test between the PMS sample and the volume-limited Raghavan et al. (2010) sample, reporting a p-value of $<10^{-4}$. The difference is statistically significant, which corroborates the visual impression that the PMS sample indeed occupies a different distribution of tertiary-to-binary orbital periods than the field-age sample.

For our Robo-AO sample, we note that the upper limits of our estimated tertiary periods (red and orange arrows in Figure 7) are consistent with the larger field-age samples of Raghavan et al. (2010) and Tokovinin (2018).

5.2. Hierarchical Unfolding

Although tertiary-induced inner binary period shortening is evident, there is growing evidence that a single mechanism, such as KCTF, cannot recreate the entire population of known close binaries (e.g., Bate 2019; Kounkel et al. 2019). As has already been shown for individual cases (e.g., Gómez Maqueo Chew et al. 2019), we find that many of the well-characterized EBs in young (<30 Myr) triple systems have already achieved close separations ($\lesssim$0.1 au). Evolution by the KCTF mechanism, which has an effective timescale on the order of $\sim$100 Myr, is unable to account for these (<30 Myr) systems.

The alternative mechanism of hierarchical unfolding (e.g., Reipurth & Mikkola 2012), in which the orbit of a newly bound wide (100–1000 au) binary is shrunk by ejecting a third body into a distant orbit, is unable to achieve the close separation of an SB alone. However, because these interactions often result in a highly eccentric orbit for the binary, the additional dissipative interactions with the primordial gas expected in the disks of these young binaries also aid in the observed orbital decay. Recent population synthesis work (Moe & Kratter 2018) found that $\sim$60% of close binaries ($P_{\rm bin} < 10$ days) form during the PMS phase and in a compact configuration with a tertiary companion as a consequence of this process.

Known PMS triples with estimated orbits are notably compact and weakly hierarchical, with significantly smaller tertiary-to-binary period ratios than the majority of known triples in the field (see Figure 7). The majority of our Robo-AO candidate triples with known ages (12/15) are field-age ($\sim$1 Gyr) systems and have thus had sufficient time to dynamically evolve. In comparison to the PMS systems, they all lie in the cluster of points with upper limit period ratios of $10^{3.5}$ or greater. Although it is not feasible to reconstruct the dynamical pathway taken by each system, as both hierarchical unfolding and KCTF are able to account for the current orbital configurations, their hierarchical nature is evident, with a range of hardened inner binaries ($P_{\rm bin} < 30$ days) and large tertiary-to-binary period ratios ($\geqslant 10^{3.5}$).

This apparent difference between the field-age and PMS sample could be equally explained from the standpoint of the tertiary companion or inner binary. The simulations of Reipurth & Mikkola (2012) found that the most extreme wide systems take on the order of $\sim$100 Myr to fully unfold, and thus it is possible that some of the tertiaries in these PMS systems still have significant dynamical evolution to undergo. Alternatively, if the reservoir of primordial circumstellar disk gas is not yet exhausted, it is possible that some of our PMS binaries are still in the process of hardening if young enough. Thus, the conditions for evolution via hierarchical unfolding with dissipative gas interactions appear to be in place for the youngest systems.

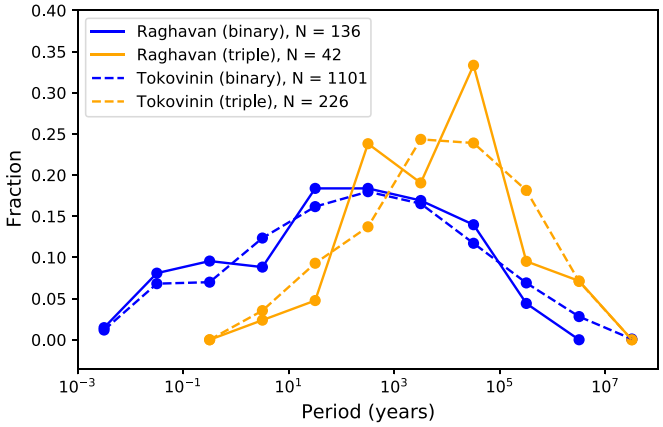

Figure 8. Distribution of orbital periods between the lone binaries (blue) and tertiaries (orange) from the volume-limited Raghavan et al. (2010; solid) and Tokovinin (2014a; dashed) samples.

Another question is whether the dynamical evolution of triple systems leads to tertiaries that are wider than would be expected to arise from the formation process alone. Tokovinin (2014b) argued that the overall distribution of inner and outer orbital periods in multiple-star systems is consistent with dynamical sculpting that produces inner binaries populating the short-period part of the overall distribution and outer companions populating the long-period part of the overall distribution. But is there evidence that tertiaries come to reach wider separations than the widest binaries? To this end, we compare the period distributions of simple binaries versus triples within the volume-limited Raghavan et al. (2010) and Tokovinin (2014a) samples (Figure 8).

The upper bound of the appropriate period range for the comparison considers the longest period for which both binaries and tertiaries are observed ($\sim 10^7$ yr). Because the inner binaries of triple systems cannot be as wide as their tertiaries, we do not extend the lower bound to the period for which the tightest tertiaries are observed (10 yr); instead, we consider the longest-period binaries in the triples identified in the larger volume-limited sample of Tokovinin (2014a). We choose a generous lower bound of 10^3 yr, with only a small number of binaries (identified through CPM) exceeding this period.

Within this period range (10^3 yr $< P < 10^7$ yr), we perform a two-sample Anderson–Darling test on the lone Tokovinin binaries versus tertiaries (dashed lines in Figure 8) to probe the differences in the tails of these distributions. We do not find strong evidence (p-value $= 0.06$) that tertiary companions find themselves at wider separations than their simple binary counterparts. We find a similar result when considering the Raghavan sample (solid lines in Figure 8). There is therefore no strong evidence to suggest that the mechanisms governing the underlying populations of the widest binaries and tertiaries are distinct, consistent with the findings of Tokovinin (2014b).

6. Summary

In this paper, we have conducted Robo-AO imaging for a sample of 60 SBs with known periods and distances. For 52 individual sources, we identify candidate companions, or a lack thereof, through a visual inspection of their PSF-subtracted

images and search for additional candidates using Gaia parallaxes, proper motion, and astrometric information. Overall, we identify 31 candidate tertiary systems and one candidate quadruple system.

A principal aim of this paper was to test the reproducibility of the canonical result from Tokovinin et al. (2006), namely that tertiary frequency is a strong function of inner binary orbital period. For our Robo-AO-identified candidate tertiaries, we find higher fractions of tertiary companions around shorter-period binaries, with 75% of $P_{\rm bin} < 3$ day systems having a tertiary companion compared to ∼47% of the longest-period ($P_{\rm bin} > 30$ days) systems, consistent with the findings of Tokovinin et al. (2006) and extending that result to even longer-period inner binaries. A separate test sample of the smaller number of Robo-AO-observed KOI EBs also shows this trend. The two samples thus appear to independently reproduce the canonical result of Tokovinin et al. (2006).

We have roughly estimated the tertiary period for each of our candidate triples, exploring the dependence of their distributions on inner SB period and age. Although we are unable to determine the prominent mechanism at work for their dynamical evolution, we note that all of our field-age Robo-AO candidate triples find themselves in hierarchical configurations with large ($P_3/P_1 > 10^{3.5}$) tertiary–binary period ratio upper limits. In comparison, we find that known young PMS triples are much more compact in comparison, with the conditions for hierarchical unfolding (e.g., Reipurth & Mikkola 2012) already in place. We find these results to be consistent with the recent population synthesis predictions of Moe & Kratter (2018).

Taken together, the results of this investigation can be interpreted through a framework in which stellar triples evolve from relatively compact configurations to increasingly hierarchical configurations in which the hardest binaries arise almost exclusively through tertiary interactions and the widest tertiaries arise through interactions with their inner binaries.

This research made use of NASA's Astrophysics Data System. This research made use of the VizieR catalog access tool and the SIMBAD database, operated at CDS, Strasbourg, France. This work made use of the IPython package (Pérez & Granger 2007), NumPy (Van Der Walt et al. 2011), and SciPy (Virtanen et al. 2020). This research made use of Astropy, a community-developed core Python package for astronomy (Astropy Collaboration et al. 2013), as well as matplotlib, a Python library for publication-quality graphics (Hunter 2007). This research made use of ds9, a tool for data visualization supported by the Chandra X-ray Science Center (CXC) and the High Energy Astrophysics Science Archive Center (HEASARC) with support from the JWST Mission office at the Space Telescope Science Institute for 3D visualization (Joye & Mandel 2003). These acknowledgments were compiled using the Astronomy Acknowledgment Generator. Finally, the authors are most grateful to the anonymous referee, whose thorough and careful review substantially improved the manuscript.

This work also made use of data from the European Space Agency (ESA) mission Gaia (https://www.cosmos.esa.int/gaia), processed by the Gaia Data Processing and Analysis Consortium (DPAC; https://www.cosmos.esa.int/web/gaia/dpac/consortium). Funding for the DPAC has been provided by national institutions, in particular the institutions participating in the Gaia Multilateral Agreement. This research made use of the crossmatch service provided by CDS, Strasbourg. This research made use of the Washington Double Star Catalog maintained at the U.S. Naval Observatory. The Robo-AO instrument was developed with support from the National Science Foundation under grants AST-0906060, AST-0960343, and AST-1207891; IUCAA; the Mt. Cuba Astronomical Foundation; and a gift from Samuel Oschin. We thank the NSF and NOAO for making the Kitt Peak 2.1 m telescope available, as well as the observatory staff at Kitt Peak (KP) for their efforts to assist Robo-AO KP operations. The authors are honored to be permitted to use astronomical data observed on Iolkam Du'ag (Kitt Peak), a mountain with particular significance to the Tohono O'odham Nation. Robo-AO KP is a partnership between the California Institute of Technology, the University of Hawai'i, the University of North Carolina at Chapel Hill, the Inter-University Centre for Astronomy and Astrophysics (IUCAA) at Pune, India, and the National Central University, Taiwan. Robo-AO KP was also supported by a grant from Sudha Murty, Narayan Murthy, and Rohan Murty; a grant from the John Templeton Foundation; and the Mt. Cuba Astronomical Foundation. In particular, we are thankful for the efforts of Christoph Baranec, Nicholas Law, Dmitry Duev, Reed Riddle, Maissa Salama, and Rebecca Jensen-Clem of the Robo-AO Kitt Peak team.

Facility: KPNO: 2.1 m (Robo-AO).

Appendix
Mosaics of Robo-AO Images

To display the candidate companions identified from our Robo-AO imaging, we first show a mosaic of our pre-PSF-subtracted images (Figures 9–11) for each SB system, followed by a mosaic of our PSF-subtracted images (Figures 12 and 13) with visual aids pointing to residual features that indicate image distortions suggestive of companions; these features are PSF residuals and do not represent resolved detections of the putative companions (see Section 2.2). Additional vetting of companions via Gaia astrometry and previous observations is described in Section 3.

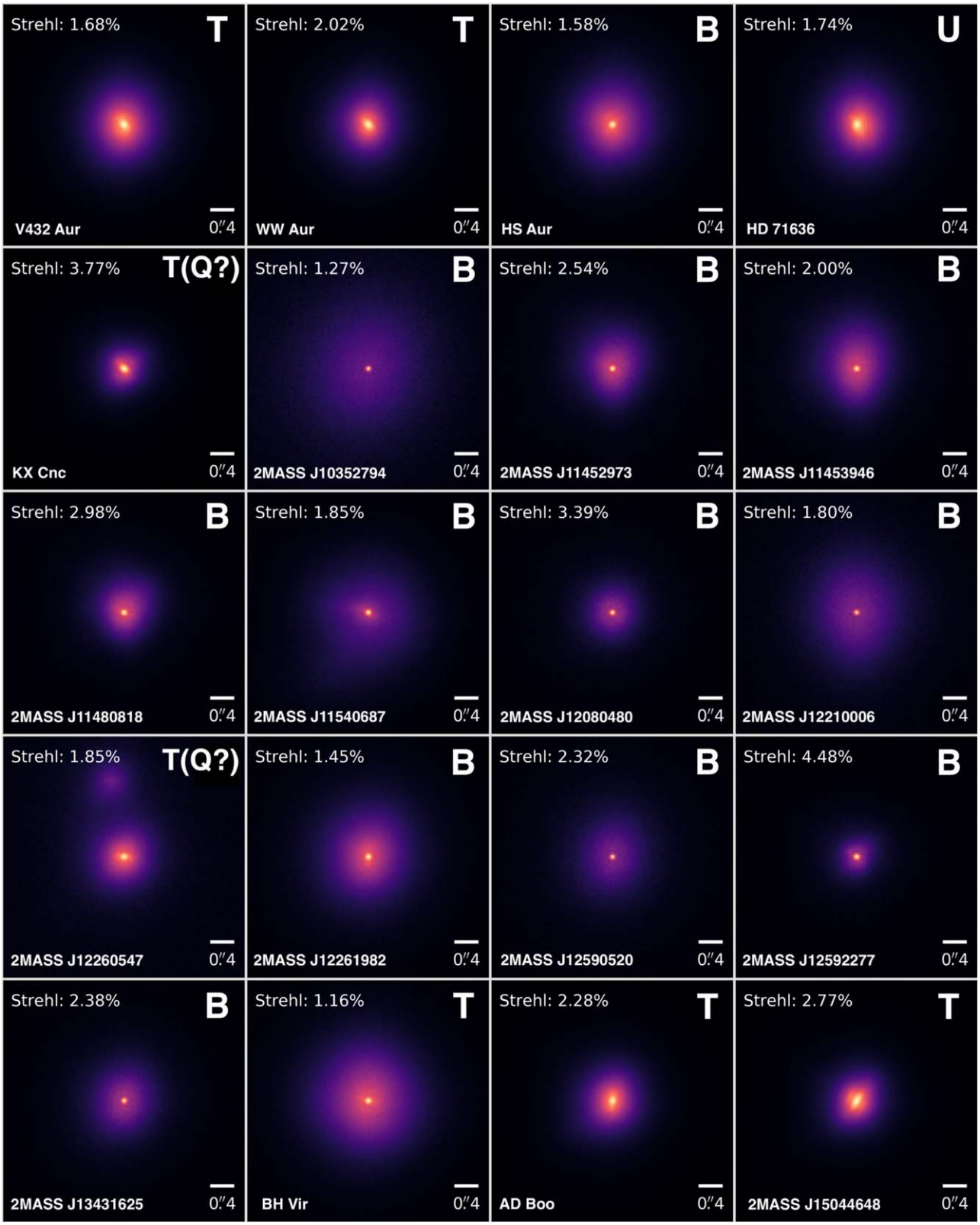

Figure 9. Pre-PSF-subtracted images for Robo-AO SBs (continued in Figures 10 and 11). We note that the designation in the top right corner of each image corresponds to that determined strictly by our Robo-AO imaging and thus does not include the results of our wide companion identifications in Section 3. Our final identifications are those listed in Table 2.

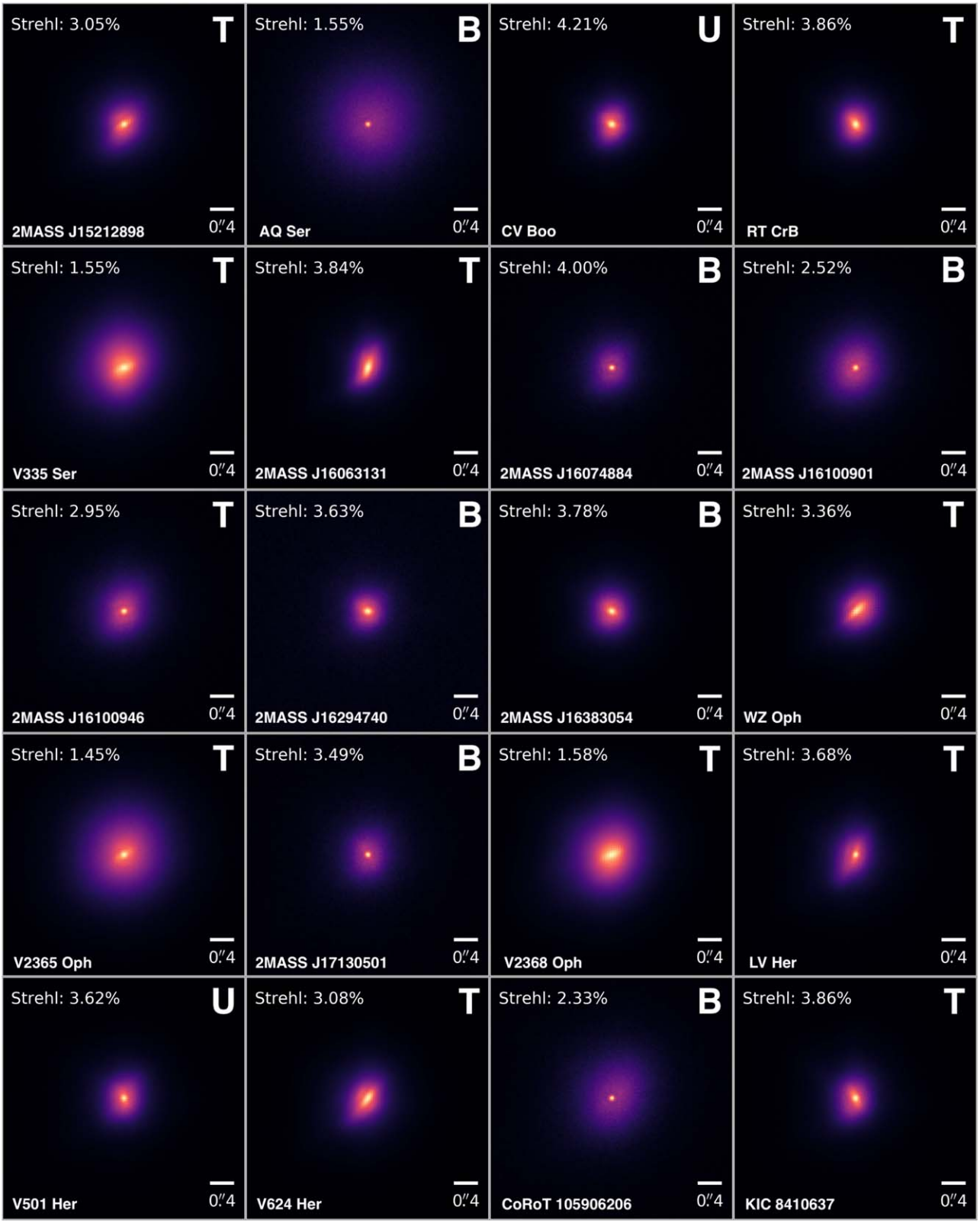

Figure 10. Pre-PSF-subtracted images for Robo-AO SBs (continued from Figure 9). We note that the designation in the top right corner of each image corresponds to that determined strictly by our Robo-AO imaging and thus does not include the results of our wide companion identifications in Section 3. Our final identifications are those listed in Table 2.

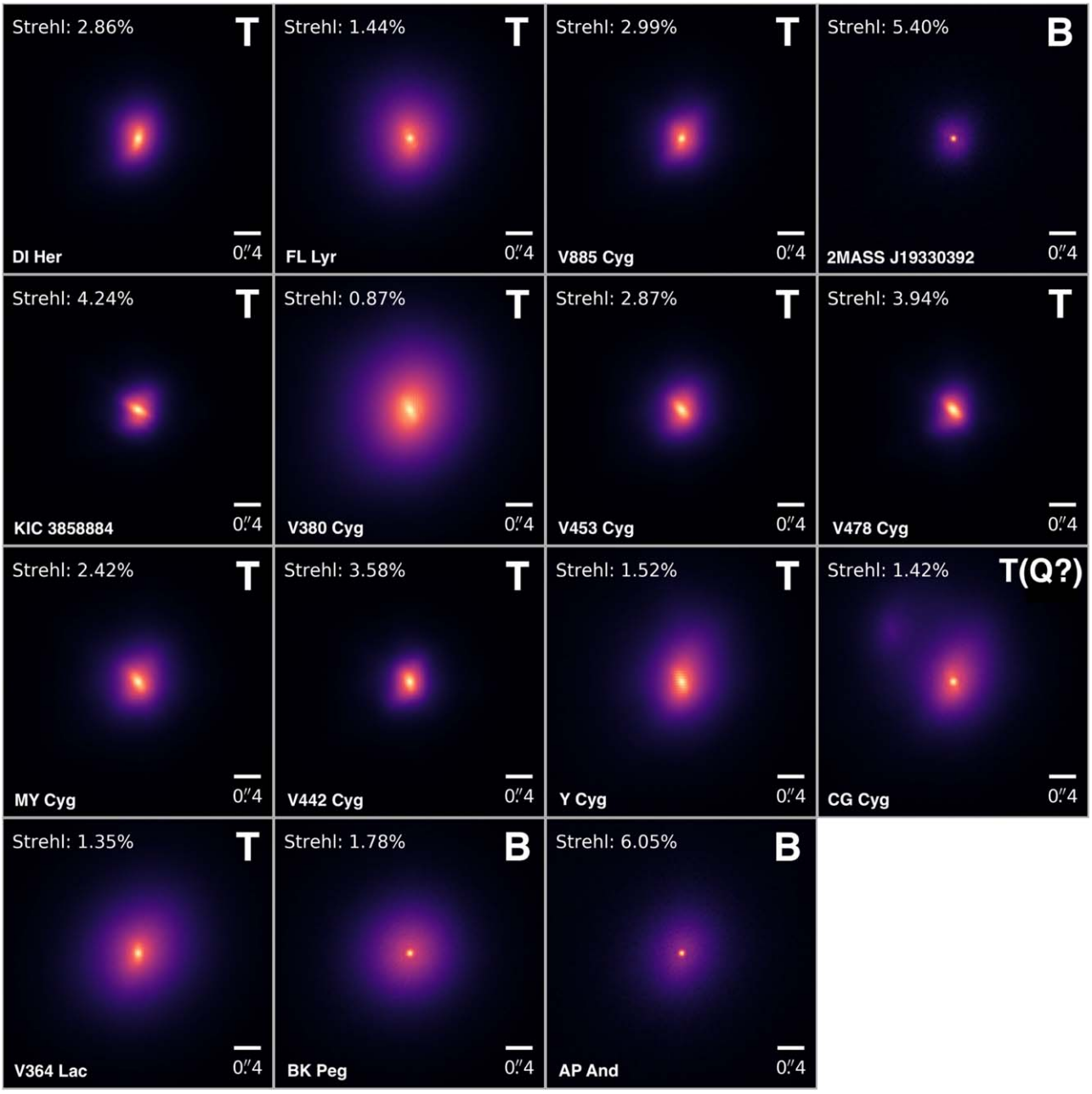

Figure 11. Pre-PSF-subtracted images for Robo-AO SBs (continued from Figure 10). We note that the designation in the top right corner of each image corresponds to that determined strictly by our Robo-AO imaging and thus does not include the results of our wide companion identifications in Section 3. Our final identifications are those listed in Table 2.

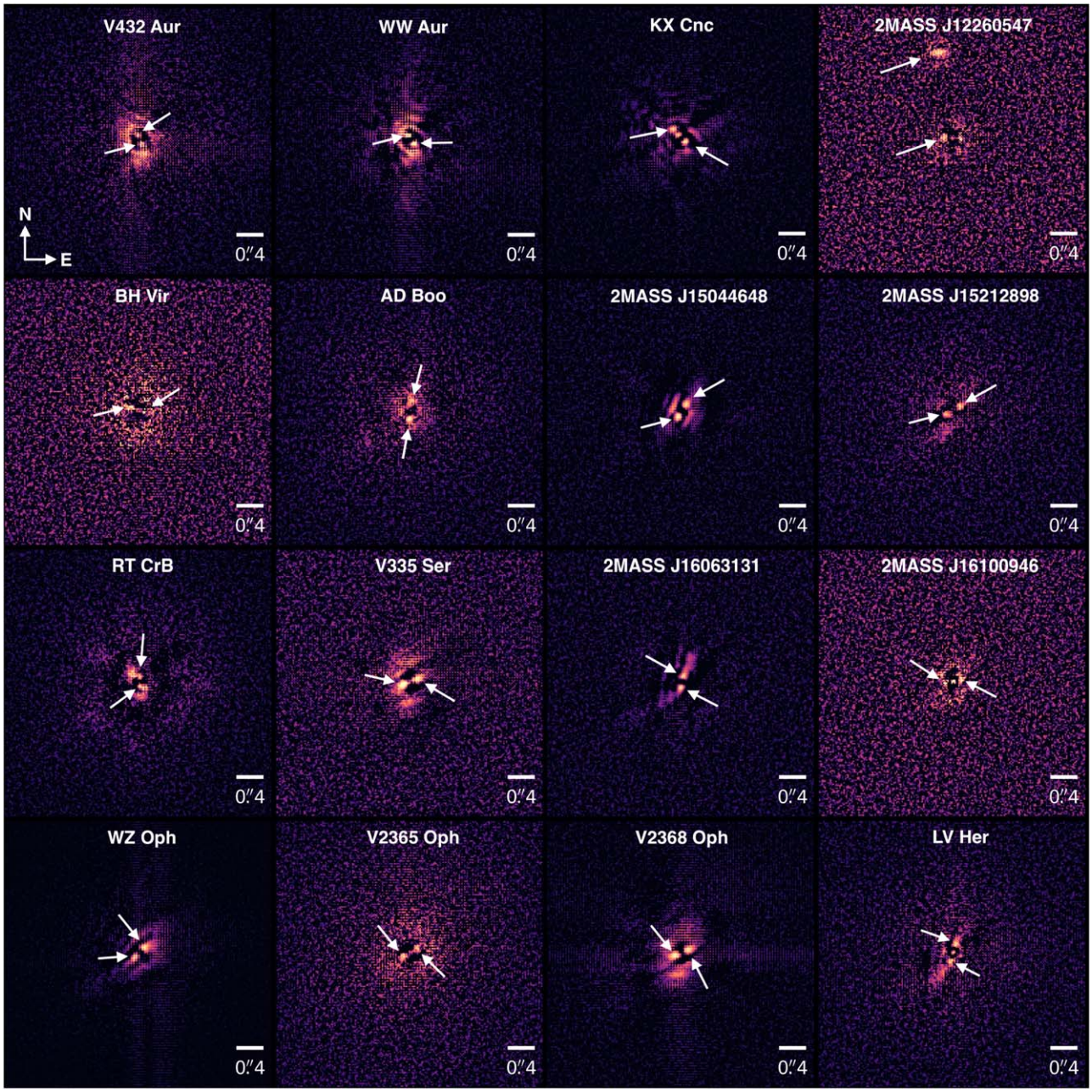

Figure 12. PSF-subtracted images for Robo-AO-identified candidate multiples (continued in Figure 13). Visual aids point to residual features that indicate image distortions suggestive of companions; these features are PSF residuals and do not represent resolved detections of the putative companions (see Section 2.2). Additional vetting of companions via Gaia astrometry and previous observations is described in Section 3.

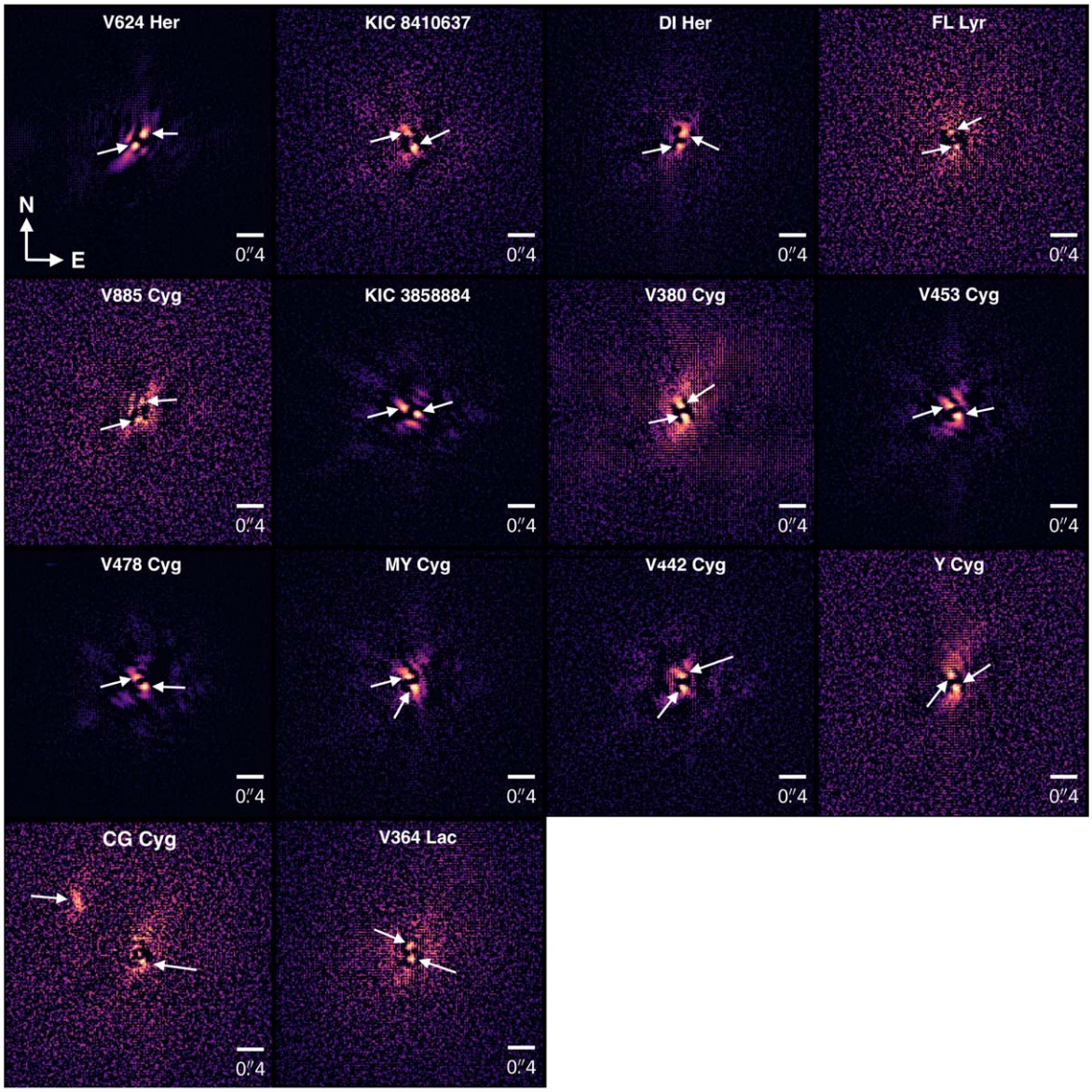

Figure 13. PSF-subtracted images for Robo-AO-identified candidate multiples (continued from Figure 12). Visual aids point to residual features that indicate image distortions suggestive of companions; these features are PSF residuals and do not represent resolved detections of the putative companions (see Section 2.2). Additional vetting of companions via Gaia astrometry and previous observations is described in Section 3.

ORCID iDs

Stefan Laos https://orcid.org/0000-0001-8407-2105
Keivan G. Stassun https://orcid.org/0000-0002-3481-9052
Robert D. Mathieu https://orcid.org/0000-0002-7130-2757

References

Alam, S., Albareti, F. D., Allende Prieto, C., et al. 2015, ApJS, 219, 12
Astropy Collaboration, Robitaille, T. P., Tollerud, E. J., et al. 2013, A&A, 558, A33
Baranec, C., Ziegler, C., Law, N. M., et al. 2016, AJ, 152, 18
Bate, M. R. 2019, MNRAS, 484, 2341
Borkovits, T., Rappaport, S. A., Hajdu, T., et al. 2020, MNRAS, 493, 5005
Coronado, J., Hełminiak, K. G., Vanzi, L., et al. 2015, MNRAS, 448, 1937
Corporon, P., Lagrange, A. M., & Beust, H. 1996, A&A, 310, 228
Czekala, I., Andrews, S. M., Torres, G., et al. 2017, ApJ, 851, 132
Deacon, N. R., Liu, M. C., Magnier, E. A., et al. 2014, ApJ, 792, 119
Eggleton, P. P., & Kiseleva-Eggleton, L. 2001, ApJ, 562, 1012
Evans, D. F. 2018, RNAAS, 2, 20
Evans, D. W., Riello, M., De Angeli, F., et al. 2018, A&A, 616, A4
Fuhrmann, K., Chini, R., Kaderhandt, L., & Chen, Z. 2017, ApJ, 836, 139
Gaia Collaboration, Brown, A. G. A., Vallenari, A., et al. 2018, A&A, 616, A1
Gaia Collaboration, Prusti, T., de Bruijne, J. H. J., et al. 2016, A&A, 595, A1
Gomez Gonzalez, C. A., Wertz, O., Absil, O., et al. 2017, AJ, 154, 7
Gómez Maqueo Chew, Y., Hebb, L., Stempels, H. C., et al. 2019, A&A, 623, A23
Guerrero, C. A., Orlov, V. G., Monroy-Rodríguez, M. A., & Borges Fernandes, M. 2015, AJ, 150, 16
Hillenbrand, L. A., Zhang, C., Riddle, R. L., et al. 2018, AJ, 155, 51
Horch, E. P., van Belle, G. T., Davidson, J. W. J., et al. 2015, AJ, 150, 151
Hunter, J. D. 2007, CSE, 9, 90
Jensen-Clem, R., Duev, D. A., Riddle, R., et al. 2017, AJ, 155, 32
Jiménez-Esteban, F. M., Solano, E., & Rodrigo, C. 2019, AJ, 157, 78
Joye, W. A., & Mandel, E. 2003, in ASP Conf. Ser. 295, Astronomical Data Analysis Software and Systems XII, ed. H. E. Payne, R. I. Jedrzejewski, & R. N. Hook (San Francisco, CA: ASP), 489
Kellogg, K., Prato, L., Torres, G., et al. 2017, ApJ, 844, 168
Knapp, W., & Nanson, J. 2018, JDSO, 14, 503
Kounkel, M., Covey, K., Moe, M., et al. 2019, AJ, 157, 196
Lafrenière, D., Marois, C., Doyon, R., & Barman, T. 2009, ApJL, 694, L148

Law, N. M., Morton, T., Baranec, C., et al. 2014, ApJ, 791, 35
Lindegren, L., Hernández, J., Bombrun, A., et al. 2018, A&A, 616, A2
Maíz Apellániz, J., & Weiler, M. 2018, A&A, 619, A180
Mardling, R. A., & Aarseth, S. J. 2001, MNRAS, 321, 398
Matijevič, G., Prša, A., Orosz, J. A., et al. 2012, AJ, 143, 123
McAlister, H. A., Hartkopf, W. I., Hutter, D. J., & Franz, O. G. 1987, AJ, 93, 688
Moe, M., & Kratter, K. M. 2018, ApJ, 854, 44
Pérez, F., & Granger, B. E. 2007, CSE, 9, 21
Prša, A., Guinan, E. F., Devinney, E. J., et al. 2008, ApJ, 687, 542
Raghavan, D., McAlister, H. A., Henry, T. J., et al. 2010, ApJS, 190, 1
Reipurth, B., & Mikkola, S. 2012, Natur, 492, 221
Riddle, R. L., Tokovinin, A., Mason, B. D., et al. 2015, ApJ, 799, 4
Roberts, L. C., & Mason, B. D. 2018, MNRAS, 473, 4497
Rucinski, S. M., Pribulla, T., & van Kerkwijk, M. H. 2007, AJ, 134, 2353
Sana, H., Le Bouquin, J.-B., Lacour, S., et al. 2014, ApJS, 215, 15
Schaefer, G. H., Prato, L., Simon, M., & Zavala, R. T. 2012, ApJ, 756, 120
Soummer, R., Pueyo, L., & Larkin, J. 2012, ApJL, 755, L28
Southworth, J. 2015, in ASP Conf. Ser. 496, Living Together: Planets, Host Stars and Binaries, ed. S. M. Rucinski, G. Torres, & M. Zejda (San Francisco, CA: ASP), 164
Stassun, K. G., Feiden, G. A., & Torres, G. 2014, NewAR, 60, 1
Stassun, K. G., & Torres, G. 2016, AJ, 152, 180
Tokovinin, A. 2014a, AJ, 147, 86
Tokovinin, A. 2014b, AJ, 147, 87
Tokovinin, A. 2018, ApJS, 235, 6
Tokovinin, A., Thomas, S., Sterzik, M., & Udry, S. 2006, A&A, 450, 681
Torres, G., Andersen, J., & Giménez, A. 2010, A&ARv, 18, 67
Troup, N. W., Nidever, D. L., Lee, N. D., et al. 2016, AJ, 151, 85
Van Der Walt, S., Colbert, S. C., & Varoquaux, G. 2011, CSE, 13, 22
Virtanen, P., Gommers, R., Oliphant, T. E., et al. 2020, NatMe, 17, 261
Woollands, R. M., Pollard, K. R., Ramm, D. J., Wright, D. J., & Böhm, T. 2013, MNRAS, 432, 327
Ziegler, C., Law, N. M., Baranec, C., et al. 2018a, AJ, 155, 161
Ziegler, C., Law, N. M., Baranec, C., et al. 2018b, AJ, 156, 83
Ziegler, C., Law, N. M., Morton, T., et al. 2017, AJ, 153, 66